INL/CON-07-12378
PREPRINT

Evaluation of Fluid Conduction and Mixing Within a Subassembly of the Actinide Burner Test Reactor

NURETH-12

Cliff B. Davis

September 2007

The INL is a
U.S. Department of Energy
National Laboratory
operated by
Battelle Energy Alliance

The 12th International Topical Meeting on Nuclear Reactor Thermal Hydraulics (NURETH-12) Log Number: 186
Sheraton Station Square, Pittsburgh, Pennsylvania, U.S.A. September 30-October 4, 2007.

EVALUATION OF FLUID CONDUCTION AND MIXING WITHIN A SUBASSEMBLY OF THE ACTINIDE BURNER TEST REACTOR

Cliff B. Davis
Idaho National Laboratory
P.O. Box 1625
Idaho Falls, ID 83415-3890
Cliff.Davis@inl.gov

ABSTRACT

The RELAP5-3D code is being considered as a thermal-hydraulic system code to support the development of the sodium-cooled Actinide Burner Test Reactor as part of the Global Nuclear Energy Partnership. An evaluation was performed to determine whether the control system could be used to simulate the effects of non-convective mechanisms of heat transport in the fluid, including axial and radial heat conduction and subchannel mixing, that are not currently represented with internal code models. The evaluation also determined the relative importance of axial and radial heat conduction and fluid mixing on peak cladding temperature for a wide range of steady conditions and during a representative loss-of-flow transient. The evaluation was performed using a RELAP5-3D model of a subassembly in the Experimental Breeder Reactor-II, which was used as a surrogate for the Actinide Burner Test Reactor.

KEYWORDS
ABTR, RELAP5-3D, Conduction, Mixing, Sodium

1. INTRODUCTION

The Actinide Burner Test Reactor (ABTR) is envisioned as a sodium-cooled, fast reactor that will burn the actinides generated in light water reactors to reduce nuclear waste and ease proliferation concerns as part of the Global Nuclear Energy Partnership. RELAP5-3D[1] is being considered as a thermal-hydraulic system code to support the development of the ABTR. An evaluation[2] of the code's applicability for modeling the ABTR indicated that non-modeled mechanisms of heat transport, including heat conduction and mixing in the fluid could be important.

An evaluation was performed to determine whether existing models in RELAP5-3D could be used to simulate the non-modeled mechanisms of heat transport. The evaluation determined the importance of axial and radial heat conduction in the fluid for a wide range of steady-state conditions and during a representative loss-of-flow transient. The evaluation also determined the importance of mixing between adjacent rings within a subassembly. The evaluation used a RELAP5-3D model of a subassembly in the Experimental Breeder Reactor-II (EBR-II) because the ABTR has not yet been designed.

Section 2 of this paper describes the EBR-II subassembly and the RELAP5-3D models used in the analysis. Section 3 describes the models for calculating the heat transport mechanisms associated with heat conduction in the fluid and radial mixing within a subassembly. Section 4 presents results from the evaluations of these heat transport mechanisms. Conclusions and references are also presented.

2. RELAP5-3D MODELS

Two RELAP5-3D models were used in this evaluation. A one-dimensional model was used to simulate the effects of axial heat conduction in the fluid. A two-dimensional model was used to simulate the effects of radial conduction and mixing.

The RELAP5-3D models were based on a model[3] of the instrumented XX09 subassembly[4] in EBR-II. The XX09 subassembly is illustrated in Figures 1 and 2. The subassembly contained 61 rods arranged in a triangular array within a hexagonal wall. The array contained 59 wire-wrapped fuel rods and two rods that were used for instrument leads. Thermocouples were used to measure fluid temperatures near the top of the active core and in the mixing section near the top of the subassembly. The fuel rods contained a long gas plenum above the top of the core to accommodate fission gas release. The "annular" thimble flow region outside of the subassembly wall provided space for control rod insertion.

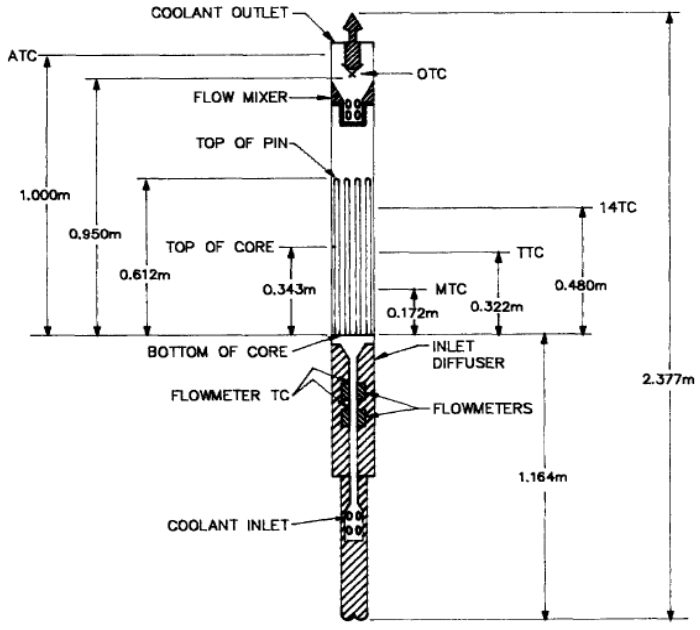

Figure 1 Schematic of the XX09 Subassembly (from Ref. 4).

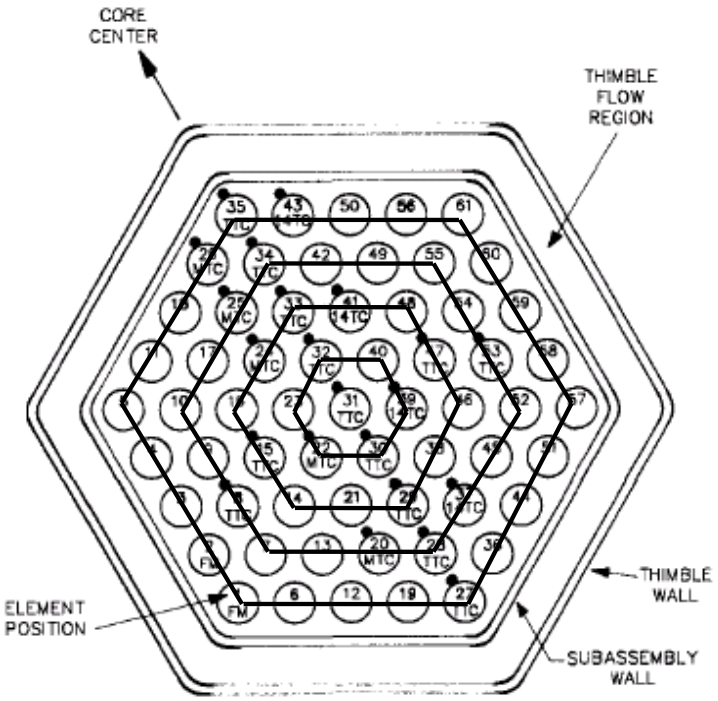

Figure 2 Cross-sectional View of the XX09 Subassembly (from Ref. 4).

The one-dimensional model of the XX09 subassembly is illustrated in Figure 3. The model represented the inlet, active core, gas plenum, thimble, and outlet regions of the subassembly. The active core was modeled with Component 140, a one-dimensional pipe that contained ten axial control volumes. Heat structures were used to represent the fuel rods and the subassembly and thimble walls. Components 100 and 220 were time-dependent volumes that specified the temperature of the sodium entering the subassembly and the pressure at the top of the subassembly. Flow boundary conditions were applied at the bottom of the subassembly with a time-dependent junction (Component 110). The flow area at Junction 190 was adjusted so that the thimble received 5% of the total flow at normal operating conditions. Reference 4 did not report the magnitude of the thimble flow, but Reference 5 stated that it was small. Reference 4 also did not describe the power profile in the XX09 subassembly or report values for the heat loss from the thimble wall to the bypass region between subassemblies. Thus, simple assumptions were made for this analysis. Specifically, the axial power profile was generated with a chopped cosine distribution with a maximum axial peaking factor of 1.2 and the radial power distribution was assumed to be uniform within the subassembly. The outer surface of the thimble wall was assumed to be adiabatic.

The RELAP5-3D model does not represent the XX09 subassembly exactly because of a lack of information about the power and flow distributions within the XX09 and adjacent subassemblies and the geometry in the inlet and outlet regions. Nonetheless, it is considered representative of a fuel subassembly in a sodium-cooled fast reactor.

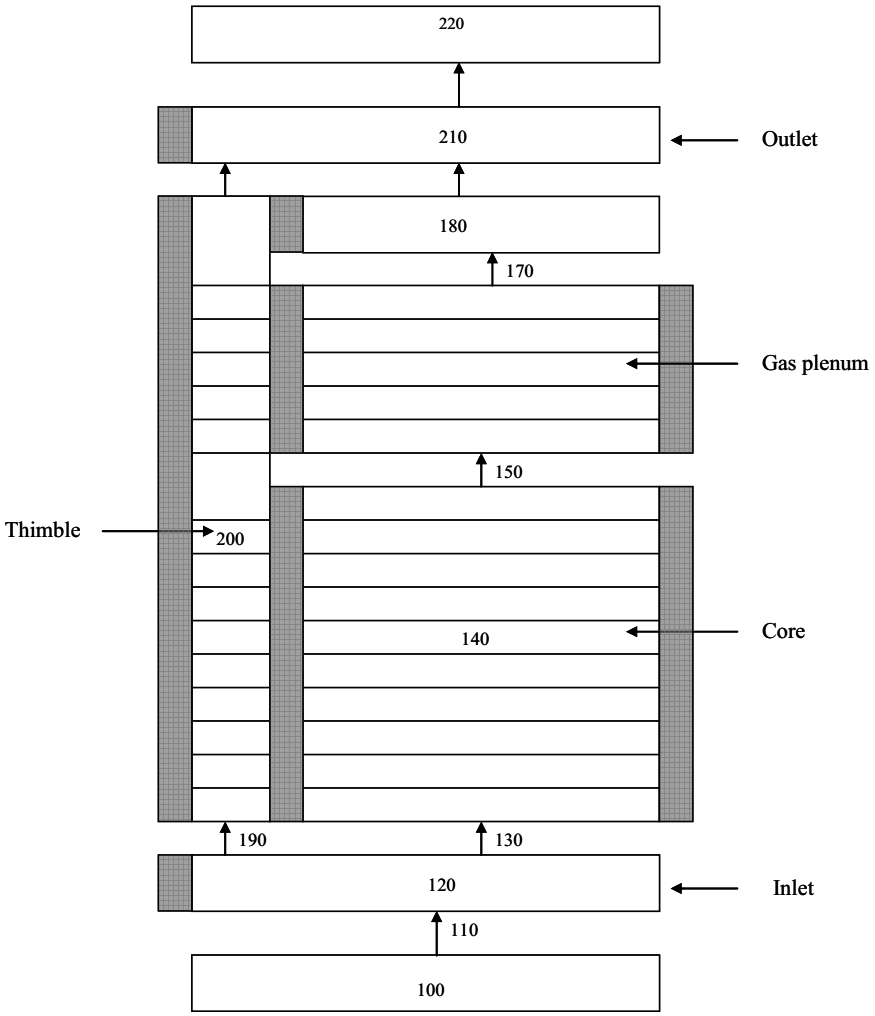

Figure 3 One-dimensional RELAP5-3D Model of the XX09 Subassembly.

A two-dimensional RELAP5-3D model of the XX09 subassembly was also developed. The two-dimensional model was identical to the one-dimensional model except that it used five parallel components to represent the core and gas plenum regions as shown in Figure 4. Each component represented one of the five hexagonal rings inside the subassembly wall shown in Figure 2. The boundaries between rings were defined by lines drawn through the center of each row of fuel rods. The five radial rings were represented by Components 141 through 145 in the core and Components 161 through 165 in the gas plenum region. Components 141 and 161 represented the first (innermost) ring, Components 142 and 162 represented the second ring, and so forth. Multiple junction components (Components 156 through 159 and 176 through 179) allowed crossflow between adjacent rings in the core and gas plenum regions.

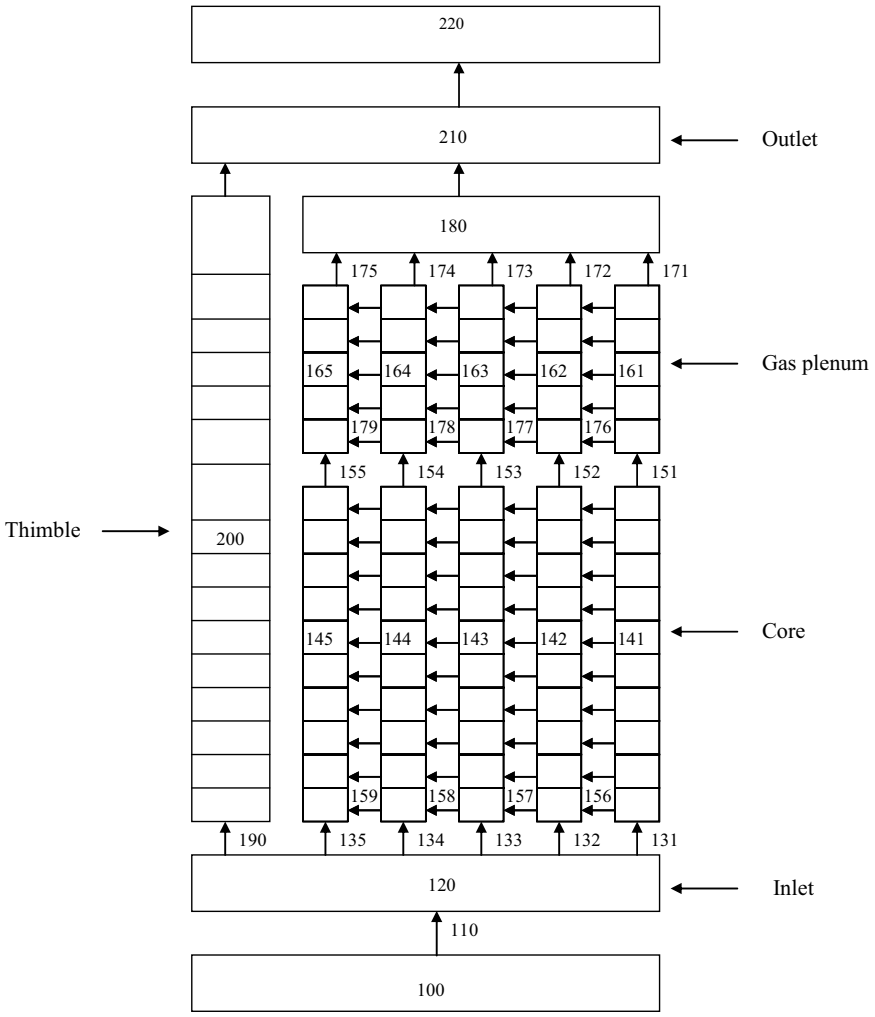

Figure 4 Two-dimensional RELAP5-3D Model of the XX09 Subassembly.

3. CONDUCTION AND MIXING MODELS

The control system model of RELAP5-3D was used to simulate the effects of fluid heat conduction and mixing. The control system provides a generalized capability to evaluate algebraic and differential equations using standard mathematical operations and functions that can interact with the code's hydrodynamic calculations. In this evaluation, the control system used fluid temperatures to calculate the heat transfer associated with heat conduction and radial mixing in the fluid. The calculated amount of power was then added to or removed from the various control volumes in the subassembly to represent these heat transport mechanisms. The model used to represent fluid conduction is described in Section 3.1. The model was initially developed for axial conduction and then was extended to represent radial conduction. Section 3.2 describes the development of the mixing model.

3.1. Fluid Conduction

RELAP5-3D was originally developed for analysis of light water reactors. The code does not represent axial or radial heat conduction in the fluid because the relatively low thermal conductivity of water ensures that their effects are small. However, the thermal conductivity of sodium is about 100 times greater than that of water. Consequently, heat conduction in the fluid has the potential to be important in fast reactors cooled by liquid sodium.

A simple rule of thumb[6] states that axial conduction may affect the heat transfer if the Peclet number is less than 100. The axial Peclet number for the XX09 subassembly in the EBR-II was about 100 at design conditions. Thus, the effects of axial conduction in the fluid could be important for fast reactors cooled by sodium, particularly during transients in which the flow decreases.

Reference 7 evaluated the effects of fluid axial conduction in the proposed STAR-LM reactor, which is cooled by the natural circulation of lead-bismuth. The relative importance of the axial conduction term was determined by choosing reference parameters and obtaining a non-dimensional energy equation, which can be written as

$$\frac{DT^{+}}{Dt^{+}} - \frac{1}{Pe^{*}} \frac{\partial^{2} T^{+}}{\partial x^{+2}} = Q_{w}^{+} \qquad (1)$$

where T is the temperature, t is time, x is the spatial coordinate, the superscript + refers to a non-dimensional parameter, and D/Dt refers to the substantial or total time derivative. The Q_w term represents wall heat transfer, the details of which are not important here. The modified Peclet number, Pe*, can be written as

$$Pe^{*} = RePr \frac{L}{D_h} \qquad (2)$$

where Re is the Reynolds number, which is based on the hydraulic diameter, D_h, Pr is the Prandtl number, and L is the length of the component. Since the traditional Peclet number is the Reynolds number times the Prandtl number, the modified Peclet number is just the traditional value times the length-to-diameter ratio.

Appropriate choices for the reference parameters result in the first and third terms in Equation 1 having an order of magnitude of one at steady state. If the modified Peclet number is of order one, the axial conduction term will also be of order one and hence will be of comparable importance to the convection term. If the modified Peclet number is 100, the axial conduction term will be roughly 1% of the convection term. Since RELAP5-3D should be able to represent second- and third-order effects, Equation 1 indicates that axial conduction in the fluid should be modeled when the modified Peclet number is less than 100.

A numerical method was developed to simulate the effects of axial conduction in the fluid. Figure 5 illustrates a simple nodalization that contains three control volumes and two junctions and defines a global distance coordinate, x. The subscripts, m-1, m, and m+1 refer to the

volumes while the subscripts m-1/2 and m+1/2 refer to the connecting junctions. The temperature, T, at the center of each volume is assumed to be known. The density, ρ, heat capacity, C, and thermal conductivity, k, are assumed to be constant within a control volume, but are allowed to vary with temperature between control volumes. The geometry is defined by the length, Δx, and flow area, A, of each volume.

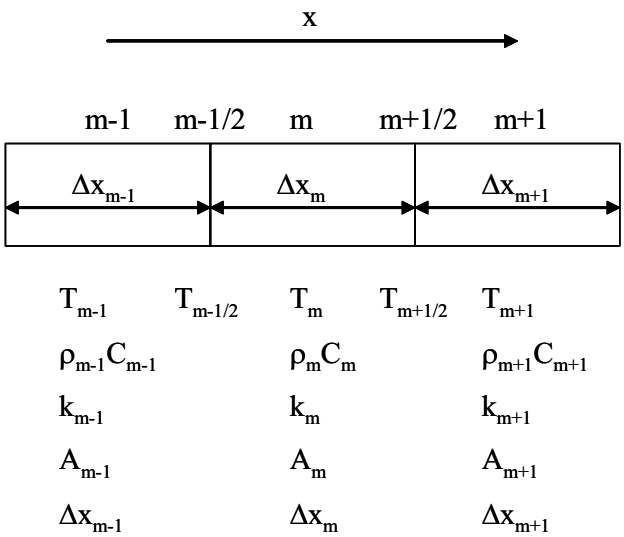

Figure 5 Nodalization Diagram for the Axial Fluid Conduction Model.

Applying Fourier's law of heat conduction to calculate the heat transfer, q, between Volume m-1 and Junction m-1/2 yields

$$q_{m-1,\,m-1/2} = -k_{m-1}A_{m-1}\frac{T_{m-1/2} - T_{m-1}}{0.5\Delta x_{m-1}} \quad . \tag{3}$$

Similarly, the heat transfer from Junction m-1/2 to Volume m is

$$q_{m-1/2,\,m} = -k_{m}A_{m}\frac{T_{m} - T_{m-1/2}}{0.5\Delta x_{m}} \, . \tag{4}$$

For convenience, a volume property, B, and a junction property, D, are defined as

$$B_m = \frac{k_m A_m}{\Delta x_m} \tag{5}$$

and

$$D_{m-1,m} = \frac{-2B_{m-1}B_m}{B_{m-1}B_m} \tag{6}$$

No energy is assumed to be stored at the junction between adjacent volumes. Therefore, Equations 3 and 4 can be equated and solved to obtain the temperature at the junction

$$T_{m-1/2} = \frac{B_{m-1}T_{m-1} + B_m T_m}{B_{m-1} + B_m} \quad . \tag{7}$$

Equations 5, 6, and 7 can be combined with either Equation 3 or 4 to obtain the heat transfer from Volume m-1 to Volume m

$$q_{m-1,m} = D_{m-1,m}(T_m - T_{m-1}) \quad . \tag{8}$$

The total power added to Volume m, Q_m, can be written as

$$Q_m = \sum_{\text{Inlets}} q_{i,m} - \sum_{\text{Outlets}} q_{m,i} \tag{9}$$

where the first sum is taken over all the junctions attached to the inlet face of Volume m and the second sum is taken over all the junctions attached to the outlet face of Volume m. The usage of the terms “inlets” and “outlets” here is governed by the global distance coordinate, x. The inlets are those junctions connected to the face of Volume m with the lower value of x while the outlets are connected to the face with the higher value of x. Hence, the definition of inlets and outlets used here differs from the normal RELAP5-3D usage, where inlets and outlets are based on the definition of positive flow according to a local coordinate that can vary for every control volume.

The RELAP5-3D control system model summarized by Equation 9 can be extended to simulate radial conduction by using appropriate values for the geometry. The length term in Equation 5 is based on the input length in the crossflow direction. The flow area term in Equation 5 is calculated as the fluid volume of the control volume divided by the input length. Since the fluid volume accounts for the presence of the fuel rods, the radial conduction model also accounts for the presence of the fuel rods in an average sense. A conduction shape factor[8] could be applied to obtain a more accurate representation of the geometrical effects on the radial heat conduction process, but was not used in this evaluation.

3.2. Radial Mixing

Each fuel rod in the XX09 subassembly was wrapped with a helical wire that maintained separation between the fuel rods and promoted mixing between subchannels. A model was developed to simulate the effects of mixing between adjacent rings in the two-dimensional model summarized in Figure 4.

The calculated mixing between rings was based on the model described in Reference 9. The transfer of energy between adjacent subchannels is based on the dimensionless effective eddy diffusivity, ε^*,

$$\varepsilon^* = \text{ effective transverse mass flux / axial mass flux } = C_m(A_{rl}/A'_l)^{1/2}\tan\theta \tag{10}$$

where

$$C_m = C_{mT} = 0.14\left(\frac{P-D}{D}\right)^{-0.5} \tag{11}$$

for turbulent flow and

$$C_m = C_{mL} = 0.077\left(\frac{P-D}{D}\right)^{-0.5} \tag{12}$$

for laminar flow. The geometrical parameters A_{r1}, A_1', and θ are calculated as

$$A_{r1} = \pi(D + D_w)D_w/6, \tag{13}$$

$$A_1' = \left(\sqrt{3}/4\right)P^2 - \pi D^2/8 \quad , \tag{14}$$

and

$$\cos\theta = H/\sqrt{H^2 + (\pi(D + D_w))^2} \quad , \tag{15}$$

where D is the diameter of the fuel rod, D_w is the diameter of the wire, P is the fuel rod pitch, and H is the height of one revolution of the helical wire wrap.

The flow regime is determined from the Reynolds number, Re, which is calculated for flow in the axial direction and accounts for the presence of the wire on the fluid velocity and the hydraulic diameter. For laminar flow,

$$Re < Re_L = 10^{1.7(P/D-1)+\log_{10}300} \quad . \tag{16}$$

For turbulent flow,

$$Re > Re_T = 10^{0.7(P/D-1)+4} \quad . \tag{17}$$

The dimensionless effective eddy diffusivity in the transition region between laminar and turbulent flow is calculated as

$$\varepsilon^* = \varepsilon^*_L + (\varepsilon^*_T - \varepsilon^*_L)\psi^{2/3} \tag{18}$$

where

$$\psi = \frac{\log_{10}Re - \log_{10}Re_L}{\log_{10}Re_T - \log_{10}Re_L} \tag{19}$$

.

The dimensionless effective eddy diffusivity accounts for the mixing caused by the wire wrapping and turbulence. The mixing caused by the wire wrapping is larger than that caused by turbulence. Based on the geometry of the XX09 subassembly, ε^* varies between 0.013 for laminar flow and 0.023 for turbulent flow.

The effective transverse mass flow, $\dot{m}_T$, between rings is calculated as

$$\dot{m}_T = \varepsilon^* G A_T, \tag{20}$$

where G is the axial mass flux and A_T is the transverse flow area, which is calculated as

$$A_T = n_{rod}(P - D)\Delta x, \tag{21}$$

where n_{rod} is the number of rods along the boundary between rings and Δx is the height of the control volume.

The effective rate of energy interchange, Q_{ij}, between rings i and j is calculated as

$$Q_{ij} = \dot{m}_T C(T_i - T_j), \tag{22}$$

where C is the specific heat capacity of the fluid and T is the fluid temperature. The values of the dimensionless effective eddy diffusivity and mass flux in Equation 20 and the heat capacity in Equation 22 are averaged from the corresponding values in the adjacent rings. The RELAP5-3D control system was used to simulate the energy exchange associated with Equation 22. The mass exchange associated with Equation 20 was not modeled directly.

4. RESULTS

4.1 Axial Conduction

The one-dimensional RELAP5-3D model shown in Figure 3 was used determine the effects of axial conduction in the fluid for a wide range of steady-state conditions and a loss-of-flow transient. The RELAP5-3D control system was used to calculate the heat transfer given by Equation 9 for all of the control volumes in the model except for the two time-dependent volumes. The model required about 7 control variables per junction to simulate axial conduction. The net power added to each volume due to axial conduction was input into the fluid using the direct heating option of the heat structures that represented the subassembly and thimble walls. Note that the net power could be either positive or negative.

A series of steady-state calculations was performed to determine the importance of axial conduction in the fluid for five operating conditions. The first operating condition corresponded to the design conditions for the XX09, which were 2.594 kg/s and 486 kW. The inlet temperature was 616 K based on the reported value for loss-of-flow tests[10] in EBR-II and was held constant for all the calculations. The other four operating conditions were performed at reduced flows and powers. The design flow and power were multiplied by the same percentage,

which varied between 10% and 0.01%, so that the same steady outlet temperature would be achieved in each case.

The flow and power boundary conditions used are illustrated in Figure 6. The model initially started with no flow and no power. The flow was ramped up to the design value over 10 s. The power was ramped up to the design value beginning at 10 s and ending at 20 s. The calculation was then continued with constant boundary conditions until steady conditions were achieved. The flow and power were then decreased by an order of magnitude in a near step change until a new steady state was achieved. This process was continued until a steady state was obtained at all of the desired operating conditions with and without axial conduction in the fluid. The modified Peclet number at the center of the core varied from about 10^4 to 1 during this process.

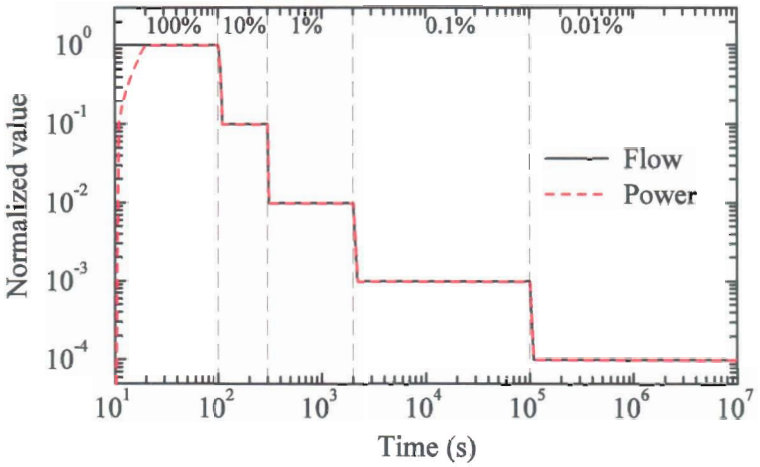

Figure 6 Flow and Power Boundary Conditions Used in the Steady-state Calculations.

Figure 7 shows steady-state axial fluid temperature profiles for the cases without axial conduction. As expected, the exit temperature was nearly the same for all of the cases because the power-to-flow ratio was the same for all the calculations. The axial temperature profiles were also nearly identical for all of the cases.

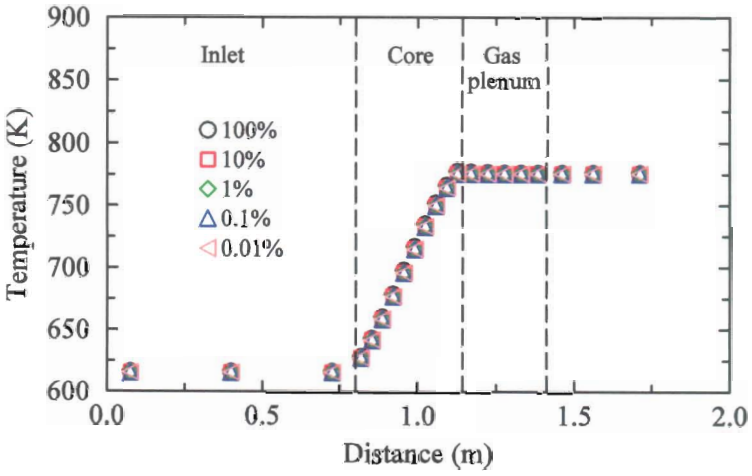

Figure 7 Fluid Temperature Profiles for the Cases without Axial Conduction.

Figure 8 shows the steady-state axial fluid temperature profiles for the cases with axial conduction. The primary effect of the axial conduction was to preheat the fluid in the inlet region, which resulted in higher temperatures in the lower core. The amount of the preheating depended on the magnitude of the flow. The maximum difference in fluid temperature due to axial conduction was 0.08 K for the 100% case, 0.3 K for the 10% case, 2 K for the 1% case, 18 K for the 0.1% case, and 95 K for the 0.01% case. Based on a comparison of Figures 7 and 8, the effects of axial conduction were nearly imperceptible until the normalized flow decreased to 0.1%.

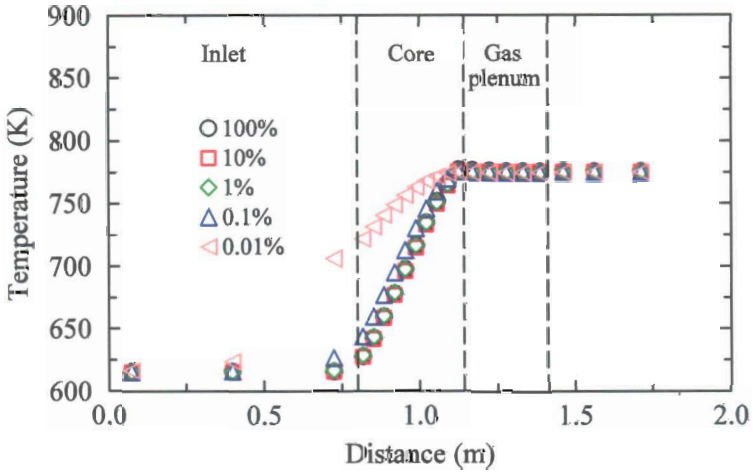

Figure 8 Fluid Temperature Profiles for the Cases with Axial Conduction in the Fluid.

The calculated effects of axial conduction shown by a comparison of Figures 7 and 8 are consistent with those expected from Equation 1. For example, the RELAP5-3D calculations indicate that the effects of axial conduction are nearly imperceptible in the 1% case. The modified Peclet number for the 1% case was about 150. Equation 1 indicates that the axial conduction term is expected to be about 0.7% of the convective term at a modified Peclet number of 150 and thus should be negligible. The RELAP5-3D calculations show that the effects of axial conduction are important for the 0.01% case, which had a modified Peclet number of 0.8. Equation 1 indicates that the axial conduction term should be slightly larger than the convective term at a modified Peclet number of 0.8, and thus clearly should be important.

The results shown in Figure 8 accounted for axial conduction in the fluid, but did not account for axial conduction in the heat structures. A review of the geometry in the core indicated that the effects of axial conduction in the fluid should be larger than those due to axial conduction through the fuel rods because the area for axial conduction in the rods is about the same as that in the coolant and the thermal conductivity of the sodium is significantly greater than the average value for the rods. The effects of axial conduction of the heat structures were quantified using the code's conduction enclosure model, which allows an approximate multi-dimensional analytical capability because the user can input a conductance that simulates axial heat transfer between adjacent heat structures. As described in Reference 11, the results of the code calculations confirmed that the effects of axial conduction in the fluid are larger than those due to axial conduction through the fuel rods.

The calculated results shown previously represented the effects of axial conduction for a wide range of steady-state conditions. Calculations were also performed that simulated a loss-of-flow transient[12] in a loop-type reactor. The transient was initiated by a loss of the primary sodium pumps, which caused a reactor scram. After the primary pumps coasted down, the pony motors held the flow at about 15% until they were assumed to fail about 5 minutes into the event. Reference 12 reported that the flow reversed in most of the core channels before the onset of natural circulation. The flow in the high-powered subassembly never reversed, but approached stagnation conditions.

The RELAP5-3D model shown in Figure 3 was used to simulate a loss-of-flow event based on the transient described in Reference 12. The normalized flow and power boundary conditions for the transient are shown in Figure 9. The inlet flow was assumed to completely stagnate for 40 s to maximize the effects of axial conduction. The power was assumed to remain constant at 2.5% of the design value for the XX09 subassembly, which is reasonably consistent with the expected decay power following infinite operation of U-235.[13] The normalized power exceeded the normalized flow for about 80 s prior to the onset of natural circulation near 440 s. The inlet fluid temperature was held constant at 616 K.

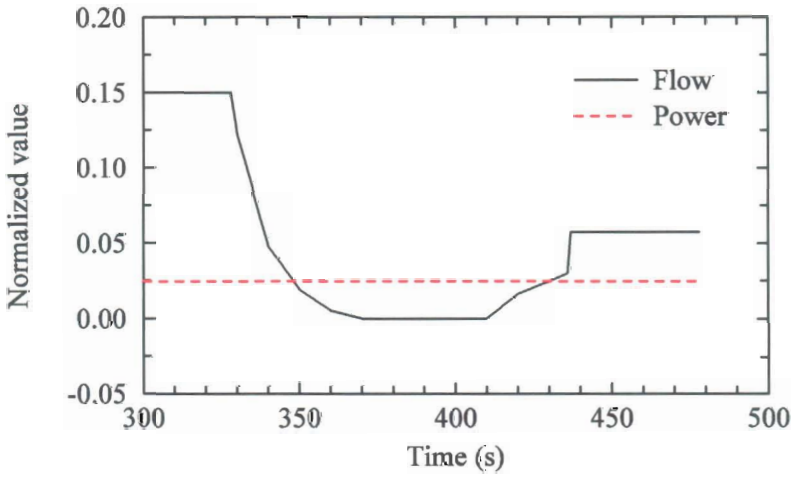

Figure 9 Boundary Conditions for the Loss-of-flow Transient.

Two calculations were performed to simulate the loss-of-flow transient after the loss of the pony motor. The calculations were started from a steady state based on the normalized flow and power shown in Figure 9 at 300 s. The first calculation neglected the effects of axial conduction in the fluid and the heat structures. The second calculation accounted for the effects of axial conduction using the control system summarized by Equation 9 to simulate the effects of conduction in the fluid and enclosure models to simulate the effects of conduction in the heat structures.

The results of the transient simulations are summarized in Figures 10 and 11, which show the maximum cladding temperature in the core as a function of time and the axial fluid temperature profile at 430 s, respectively. Axial conduction raised the temperature at the bottom of the core

and lowered the temperature at the top of the core, but the effects were relatively small. The largest difference in maximum cladding temperature was 16 K. The effect of axial conduction was exaggerated by the assumption of complete flow stagnation at the inlet to the subassembly and by the use of the one-dimensional model, which does not allow internal natural circulation within the subassembly. As will be shown later, internal natural circulation is an important cooling mechanism at low flows.

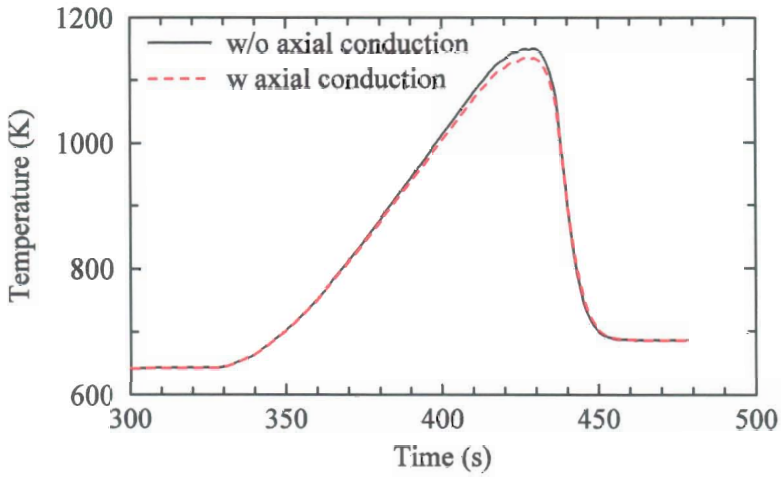

Figure 10 Maximum Cladding Temperature during the Loss-of-flow Transient.

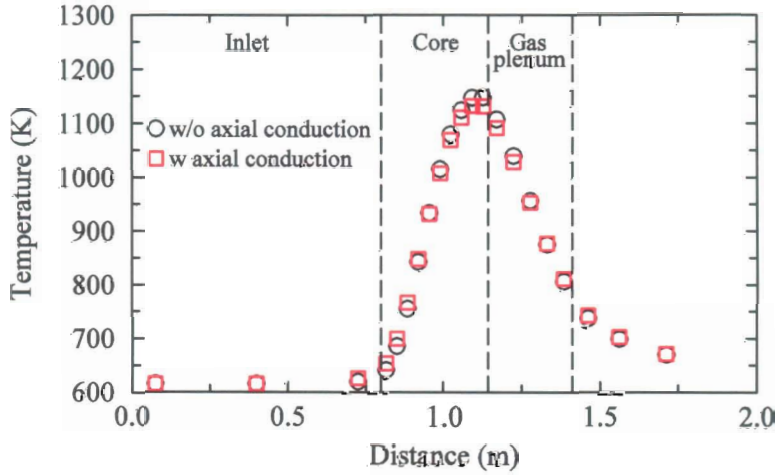

Figure 11 Axial Fluid Temperature Profiles during the Loss-of-flow Transient.

Reference 14 presents a closed-form solution for one-dimensional transient heat conduction in a solid with constant thermal properties that is bounded by two parallel planes. Graphical results are presented for a solid that is at a uniform initial temperature and subjected to a step change in temperature at both surfaces, which are also applicable for the case in which the temperature at one surface experiences a step change and an artificial surface at the midpoint of the solid is

adiabatic. Based on the geometry of the XX09 subassembly and the thermal properties of sodium, 190 s are required for 5% of the step change in temperature at one end of the core to reach the other end. The time required for 95% of the step change to propagate through the core is more than 2500 s. Since the duration of flow stagnation in the transient was only 40 s, it is not surprising that the effects of axial conduction are small during the transient.

A direct examination of the energy equation also confirms the fact that the axial conduction term is small compared to the transient term during the flow stagnation. The one-dimensional energy equation can be written as

$$\rho C \frac{\partial T}{\partial t} + \rho C v \frac{\partial T}{\partial x} - k \frac{\partial^2 T}{\partial x^2} = Q_w , \qquad (23)$$

where v is the fluid velocity, Q_w is the power per unit volume that is added to the coolant from the walls, and the other variables are as defined in Section 3. An evaluation of Equation 23 based on the geometry of the XX09 subassembly showed that the first and last terms were dominant during the flow stagnation and that the second and third terms were more than an order of magnitude smaller. Consequently, the effect of axial conduction on the peak cladding temperature is small compared to the temperature rise during the transient.

4.2 Radial Heat Transport

Radial fluid temperature measurements presented in Reference 4 showed variations of nearly 100 K near the top of the EBR-II XX09 subassembly during normal operation. Consequently, evaluations were performed to determine the importance of radial heat transport due to conduction and mixing. The evaluations utilized the two-dimensional RELAP5-3D model shown in Figure 4.

Calculations were performed both with and without the radial heat transport models summarized by Equations 9 and 22 for the sixty crossflow junctions illustrated in Figure 4 in the core and gas plenum regions. The radial conduction and mixing models required about 8 and 15 control variables per junction, respectively. Artificial heat structures were added to the inner four rings of the model so that the net power added to each volume due to radial heat transport could be accounted for using the code's direct moderator heating option. The artificial heat structures, which were only used in the calculations with radial conduction and radial mixing, were small. Their thermal capacitance was only 1% of that of the cladding in the corresponding control volume, so that they would not excessively affect calculated results during transients. The effects of axial conduction in the fluid and heat structures were neglected. The calculations that used the radial conduction model did not utilize the radial mixing model and vice versa so that the influences of each heat transport mechanism could be distinguished.

The five steady-state calculations described previously in the evaluation of axial conduction were repeated with the two-dimensional RELAP5-3D model. Figure 12 shows calculated radial temperature profiles at the top of the core for normalized flows and powers varying between 100% and 0.01% of the design values. These results were obtained without radial conduction in the fluid or radial mixing. The radial variation in temperature was large for the 100% and 10%

cases, with a maximum value of about 130 K between the first and last rings. The large radial variation in fluid temperature was primarily caused by differences in the power-to-flow ratios. The mass flow rate in each ring was nearly proportional to the flow area of the ring. In the inner four rings, the power-to-flow ratio was relatively high because the fluid was heated by fuel rods on both the inner and outer boundaries. In the outermost ring, the power-to-flow ratio was about half of that in the inner rings because the subassembly wall was unheated. Cooling of the outermost ring by the flow through the thimble region also contributed to the radial temperature variation. The radial temperature profiles were nearly flat when the normalized power and flow were 1% or less of the design values. For these cases, buoyancy enhanced the flow through the interior rings and reduced the flow in the outermost ring, which flattened the radial temperature profile. For the 100% and 10% cases, buoyancy effects were insignificant compared to the frictional effects.

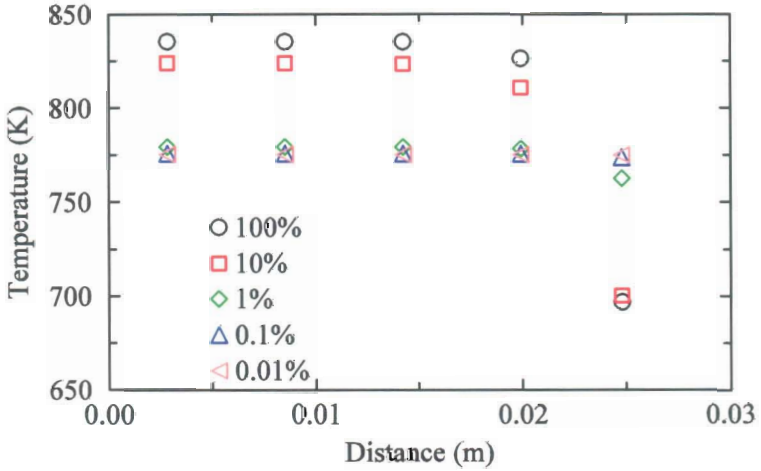

Figure 12 Steady-state Radial Fluid Temperature Profiles at the top of the Core.

The relative effects of the various models are compared in Figures 13 through 15, which show radial fluid temperature profiles at the top of the core. Figures 13 and 14 show that the maximum fluid temperature was nearly the same for all calculations with the two-dimensional model when the normalized flow and power were 10% or more. However, radial conduction in the fluid and radial mixing between rings flattened the temperature profile. These radial heat transport mechanisms reduced the temperature in the fourth ring and increased the temperature in the fifth ring. The effective conductance for radial conduction ($-D_{m-1,m}$ in Equation 6) was about four times bigger than the corresponding value for radial mixing ($\dot{m}_T C$ in Equation 22) at 100% power and flow. Consequently, radial mixing had a larger effect on the temperature profile than radial conduction at full power and flow. However, the effect on the temperature profile was reversed at 10% power and flow, with conduction more important than mixing. The relative importance of the mixing term decreased because the effect of mixing is roughly proportional to the axial flow, which was a factor of 10 lower in the 10% case. The conduction and mixing terms did not significantly affect the temperature profile when the normalized power and flow were less than or equal to 1% because the energy transport within the subassembly was dominated by internal natural circulation.

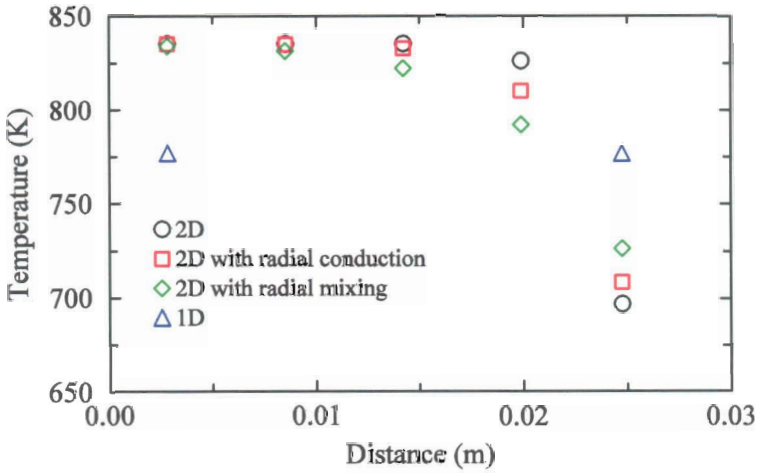

Figure 13 Radial Fluid Temperature Profiles for a Normalized Flow and Power of 100%.

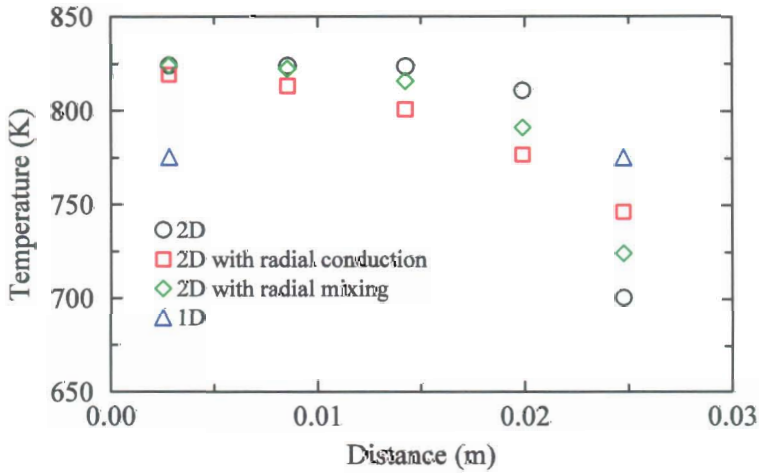

Figure 14 Radial Fluid Temperature Profiles for a Normalized Flow and Power of 10%.

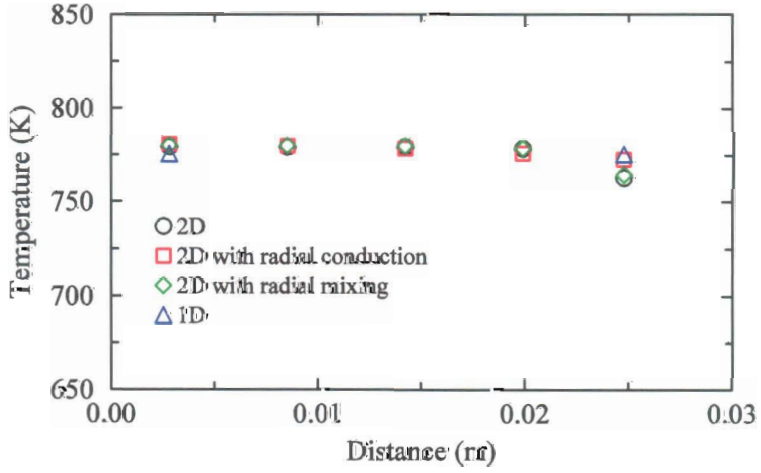

Figure 15 Radial Fluid Temperature Profiles for a Normalized Flow and Power of 1%.

Figures 13 and 14 show that the one-dimensional model under predicted the maximum fluid temperature for the 100% and 10% cases by about 50 K. Thus, the one-dimensional model would also under predict the maximum cladding temperature by about 50 K during normal operation. The one-dimensional model provides a good estimate of the maximum cladding temperature at the lower flow rates when the temperature profile is relatively flat, but of course does not account for the natural circulation within the subassembly.

Figures 16 and 17 show the relative effects of the various models on the axial fluid velocity profiles at the top of the core. All the two-dimensional models predicted a relatively flat velocity profile at 100% flow, with the largest velocity occurring in the outermost ring because of its larger hydraulic diameter. These results indicate that the velocity profile during normal operation is dominated by friction effects. The two-dimensional model without radial conduction and mixing predicted much steeper radial gradients when the normalized power and flow were 1% of the design values. In this case, the velocity profile was dominated by buoyancy effects. The velocity was lowest in the outermost ring, which was heated by only one row of rods instead of two rows for the inner rings. Figure 17 shows that radial heat conduction flattened the velocity profile significantly, but the effect of radial mixing was small.

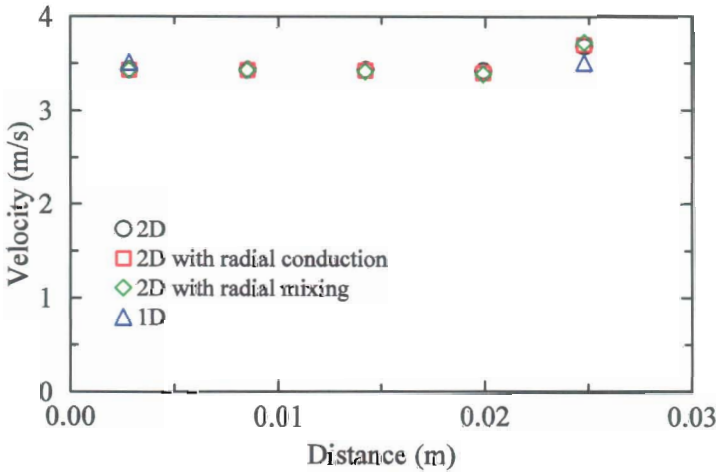

Figure 16 Axial Fluid Velocity Profiles for a Normalized Flow and Power of 100%.

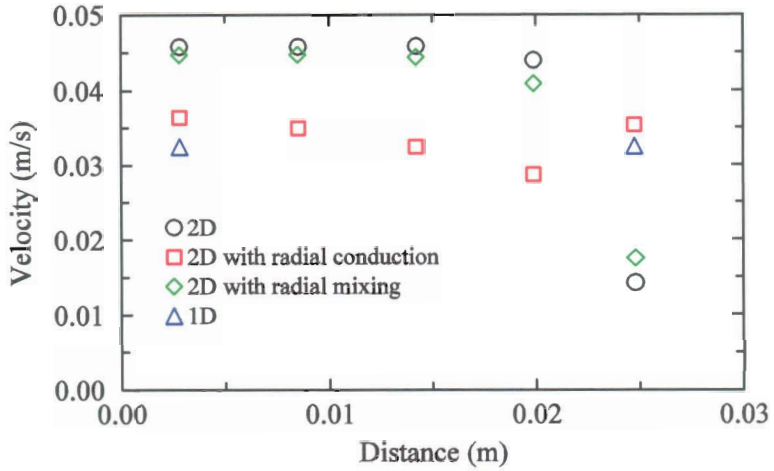

Figure 17 Axial Velocity Profiles for a Normalized Flow and Power of 1%.

The loss-of-flow transient described in Section 4.1 was also simulated using the two-dimensional RELAP5-3D model summarized in Figure 4. Figure 18 shows the effect of the radial conduction and mixing models on the maximum cladding temperature in the core. The location of the maximum temperature varied during the transient, but was always located in the inner ring and in the upper third of the core. The figure also shows results from the one-dimensional model without axial conduction that were shown previously in Figure 10.

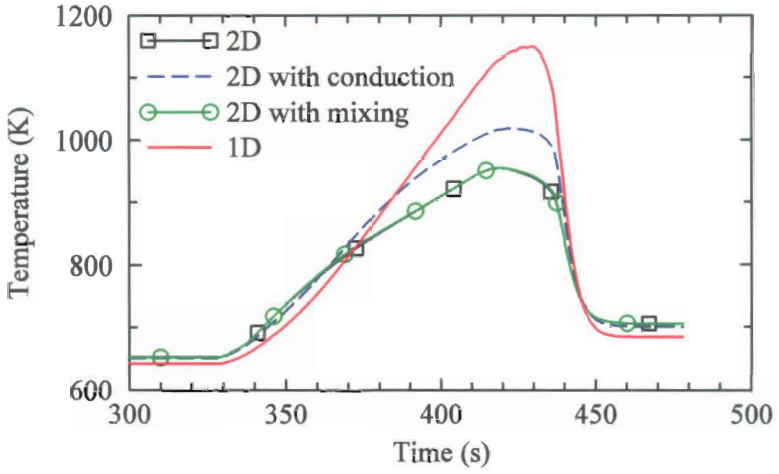

Figure 18 The Effects of Radial Heat Transport Mechanisms on the Maximum Cladding Temperature during the Loss-of-flow Transient.

The maximum cladding temperatures predicted by the two-dimensional models were about 10 K higher that from the one-dimensional model prior to the loss of the pony motor near 330 s, but the one-dimensional model predicted the highest cladding temperature during the transient by a large margin. The peak value predicted with the two-dimensional model without radial heat transport was 200 K lower than the one-dimensional result because of the mixing within the subassembly due to the buoyancy-driven flows. The higher flow rates with the two-dimensional models also resulted in cooler fluid reaching the top of the core sooner after the inlet flow restarted, which resulted in an earlier peak temperature. The effect of radial mixing was

insignificant because the amount of mixing is proportional to the axial flow rate, which was relatively small during the loss-of-flow transient. The calculated peak cladding temperature with radial conduction in the fluid was 66 K higher than the calculation without radial conduction. Radial conduction by itself would tend to flatten the radial temperature profile, which should result in a lower peak cladding temperature during a transient. However, the flatter temperature profile also reduced the natural circulation flow inside the subassembly as shown by Figure 19. The reduced flow with radial conduction caused higher temperatures in the core and lower temperatures in the gas plenum. The flow was initially upwards through the entire core in all of the calculations. However, the flow in the outermost ring reversed shortly before and returned positive shortly after the inlet flow, shown previously in Figure 9, stagnated in the two-dimensional calculations. This reverse flow in the outermost ring allowed the gas plenum and core regions to mix during the flow stagnation and was responsible for the lower cladding temperatures with the two-dimensional models.

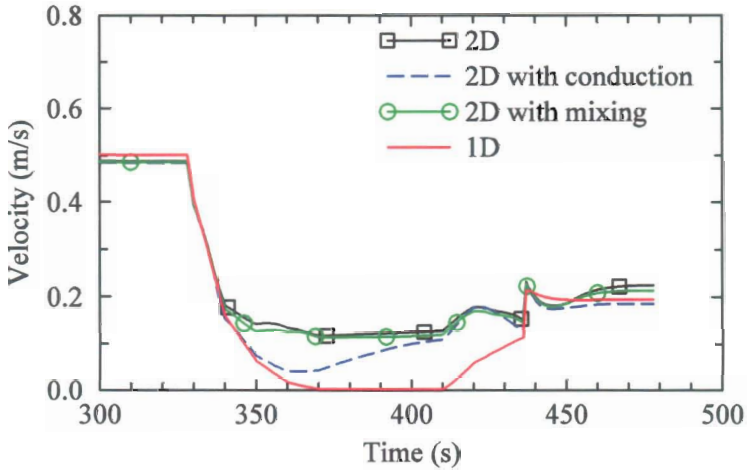

Figure 19 The Effects of Radial Heat Transport Mechanisms on the Axial Fluid Velocity at the top of the Core in the Third Ring during the Loss-of-flow Transient.

Radial conduction in the fluid significantly affected the results during the loss-of-flow transient, which was in sharp contrast to the results obtained previously with axial conduction. The fact that radial conduction significantly affects transient results is consistent with theoretical considerations. Reference 14 presents a closed-form solution for the one-dimensional temperature distribution across a solid cylinder with a constant initial temperature that is subjected to a step change in the temperature at the outer surface for the case with constant thermal properties. The closed-form solution was applied to a solid cylinder with a radius equal to that of the XX09 subassembly and with heat transfer properties that are representative of sodium. The time required for 95% of the step change to propagate to the interior of the cylinder was only 7 s. Since the duration of flow stagnation in the transient was 40 s, it is not surprising that the effects of radial conduction were significant.

4.3 Stability

The fluid conduction model summarized in Equation 9 utilizes old-time temperature values and is an explicit numerical scheme. Explicit solutions to the heat conduction equation in solids have a numerical stability limit (see Ref. 14) that can be represented as

$$\Delta t \le \frac{\rho C \Delta x^2}{2k} \tag{27}$$

where Δt is the time step size. Based on the thermal properties of sodium and the node sizes for the XX09 subassembly in the RELAP5-3D model, the stability limit is about 10 s for axial conduction and 0.25 s for radial conduction. These values are greater than the time step size typically used with RELAP5-3D during transients. A finer nodalization than used here would reduce the maximum allowed time step size and thus could be of concern with respect to stability. However, there is a large margin with respect to the axial nodalization. The radial nodalization of one ring per row of rods used in this evaluation is probably the most detailed radial nodalization that would ever be used with RELAP5-3D. Thus, an explicit numerical scheme is expected to be acceptable for representing heat conduction in the fluid in RELAP5-3D.

5. CONCLUSIONS

The effects of axial conduction in the fluid are not important for most ABTR applications. Axial conduction did not noticeably affect the steady-state temperature profiles until the normalized flow and power decreased to 0.1% of the design values. The calculated effects of axial conduction were large when the normalized power and flow were 0.01% of the design values. The effects of axial conduction during the loss-of-flow transient were relatively small because of the short time periods involved. Even though the calculated effects of axial conduction were relatively small, they were probably overstated because the analyses were performed with the one-dimensional model, which neglected the internal flows caused by buoyancy effects. If the two-dimensional model had been used, it is expected that the effects of internal natural circulation would have overwhelmed the effects of axial conduction when the normalized power and inlet flow were less than or equal to 1% of the design values.

Subchannel effects within the subassembly are important in the calculation of peak cladding temperature in the ABTR. The two-dimensional RELAP5-3D model predicted more than 100 K radial variations in fluid temperature at the top of the core during normal operation, primarily because the outermost ring was bounded by an unheated subassembly wall. The one-dimensional model underestimated the maximum fluid temperature in the subassembly by more than 50 K during normal operation. During a loss-of-flow transient, the one-dimensional model did not account for the internal recirculation due to buoyancy and thus neglected an important cooling mechanism. As a result, the peak cladding temperature obtained with the one-dimensional model was more than 130 K higher than the corresponding values from the two-dimensional models.

The effects due to radial conduction in the fluid are also important in the calculation of peak cladding temperature for the ABTR. Radial conduction significantly affected the steady-state radial temperature profile when the normalized power and flow were 10% or more of the design values. Radial heat conduction increased the peak cladding temperature by about 60 K during a loss-of-flow transient.

The effects of radial mixing in a subassembly are also important at high flow rates. The steady-state analyses showed that the mixing between subassemblies affected the radial fluid temperature profile more than radial conduction did at design conditions. The effect of mixing on the peak cladding temperature during a loss-of-flow transient was small because the amount of mixing was proportional to the axial flow rate, which was small during the event. The effects of radial mixing are expected to be important during transients with high flow rates.

Although RELAP5-3D does not have internal code models to represent heat conduction within a fluid or radial mixing between subchannels, both phenomena can be adequately simulated using the code's control system model. However, the control system approach has two limitations. First, this approach places a burden on the user in terms of the amount of work required to represent these phenomena. Internal code models that could be easily turned on or off would be far easier to use than developing a control system for each new application. Second, the control system approach places an upper limit on the number of junctions at which radial heat transport can be modeled. Because of the finite number of control variables available, radial conduction and mixing can be simulated for a maximum of about 430 junctions. Therefore, internal code models that calculate the effects of heat conduction and mixing in the fluid should be added to RELAP5-3D to support analyses of the ABTR.

ACKNOWLEDGMENTS

Work supported by the U.S. Department of Energy, Assistant Secretary for Nuclear Energy, under DOE Idaho Operations Office Contract DE-AC07-99ID13727.

NOMENCLATURE

A	Flow area
A_T	Transverse flow area
C	Heat capacity
C_m	Mixing constant
D	Fuel rod diameter
D_h	Hydraulic diameter
D_w	Wire diameter
G	Mass flux
H	Wire wrap revolution height
k	Thermal conductivity
L	Length
$\dot{m}_T$	Transverse mass flow rate
P	Fuel rod pitch
Pe	Peclet number
Pe^*	Modified Peclet number
Re	Reynolds number
q	Heat transfer rate
Q	Total heat transfer rate
Q_w	Heat transfer rate per unit volume
t	Time
T	Temperature
v	Fluid velocity
x	Spatial coordinate
ε^*	Effective eddy diffusivity
ρ	Density
Ψ	Interpolating parameter

Subscripts

L Laminar
T Turbulent

Superscripts

\+ Dimensionless parameter

REFERENCES

1. RELAP5-3D Development Team, *RELAP5-3D Code Manual Volume 1: Code Structure, System Models and Solution Methods*, Idaho National Laboratory, INEEL-EXT-98-00834, Revision 2.3, April 2005.
2. C. B. Davis, *Applicability of RELAP5-3D for Thermal-Hydraulic Analyses of a Sodium-Cooled Actinide Burner Test Reactor*, Idaho National Laboratory, INL/EXT-06-11518, July 2006.
3. J. Talley, "Modeling EBR-II Loss of Flow and Loss of Heat Sink without SCRAM using RELAP5-3D," *2006 International RELAP5 Users Seminar*, West Yellowstone, MT, September 16-18, 2006.
4. N. C. Messick, P. R. Betten, W. F. Booty, L. J. Christensen, R. M. Fryer, D. Mohr, H. P. Planchon, and W. H. Radtke, "Modification of EBR-II Plant to Conduct Loss-of-Flow-without-SCRAM Tests," *Nuclear Engineering and Design*, **101**, 13-23 (1987).
5. F. E. Dunn, J. E. Cahalan, D. Hahn, and H. Jeong, 2006, "Whole Core Sub-Channel Analysis Verification with the EBR-II SHRT-17 Test," *Proceedings of ICAAP'06*, Reno NV, June 4-8, 2006, Paper 6364.
6. W. M. Kays and M. E. Crawford, *Convective Heat and Mass Transfer*, Second Edition, McGraw-Hill Book Company, New York USA (1980).
7. Y. J. Yoo, P. Sabharwall, J. N. Reyes, Q. Wu, and J. J. Sienicki, "Effects of Fluid Axial Conduction on Liquid Metal Natural Circulation and Linear Stability," *2003 ANS/ENS International Winter Meeting, (Global 2003)*, New Orleans, LA, November 16-20, 2003, pp. 1523-1530.
8. H. Y. Jeong, K. S. Ha, Y. M. Kwon, Y. B. Lee, D. Hahn, J. E. Cahalan, and F. E. Dunn, "Evaluation of the Conduction Shape Factor with a CFD Code for a Liquid-metal Heat Transfer in Heated Triangular Rod Bundles," *Nuclear Engineering and Design*, Article in Press (2007).
9. S. K. Cheng and N. E. Todreas, "Hydrodynamic Models and Correlations for Bare and Wire-wrapped Hexagonal Rod Bundles – Bundle Friction Factors, Subchannel Friction Factors and Mixing Parameters," *Nuclear Engineering and Design*, **92**, pp. 227-251 (1986).
10. D. Mohr, L. K. Chang, E. E. Feldman, P. R. Betten, and H. P. Planchon, "Loss-of-Primary-Flow Without-Scram Tests: Pretest Predictions and Preliminary Results," *Nuclear Engineering and Design*, **101**, pp. 45-56 (1987).
11. C. B. Davis, *Evaluation of the Use of Existing RELAP5-3D Models to Represent the Actinide Burner Test Reactor*, Idaho National Laboratory, INL/EXT-07-12228, February 2007.
12. F. E. Dunn and F. G. Prohammer, "SASSYS Analysis of Degraded Shut-Down Heat Removal Performance in LMFBRs," ASME Paper No. 82-WA/HT-37 (1982).
13. American Nuclear Society, "Decay Heat Power in Light Water Reactors," *ANSI/ANS-5.1* (1979).

14. H. S. Carslaw and J. C. Jaeger, *Conduction of Heat in Solids*, Second Edition, Oxford University Press, London UK (1959).